INSTITUTE OF PHYSICS PUBLISHING INVERSE PROBLEMS

Inverse Problems **20** (2004) 1691–1711 PII: S0266-5611(04)75334-4

Imaging that exploits multipath scattering from point scatterers

Margaret Cheney[1] **and Robert J Bonneau**[2]

[1] Department of Mathematical Sciences, Rensselaer Polytechnic Institute, Troy, NY 12180, USA
[2] AFRL/SNRT, 26 Electronics Pkwy., Rome, NY 13441-4514, USA

Received 27 January 2004, in final form 28 July 2004
Published 20 August 2004
Online at stacks.iop.org/IP/20/1691
doi:10.1088/0266-5611/20/5/023

Abstract

This paper develops a method for making an image of an object when there are extra point-like scatterers in the environment. Once the location of these scatterers is known, they can be exploited in the imaging process. Here the extra point scatterers are assumed to lie between the sensor and the object of interest. A single-scattering model is used for the object itself. Detailed analysis is carried out for the case of a single extra scatterer in the foreground; the extension to the case of many scatterers is expected to be similar.

1. Introduction

Standard linear imaging methods [2, 3, 6, 22, 26] often treat the object to be imaged as a singular feature in a smooth known background. However, when the known background also contains singular features, the extra reflections can give more information about the region of interest [14, 18, 19]. This is because the extra reflections give rise to waves that probe the region from different directions.

In this paper we consider the case in which extra point-like reflectors are present in the area between the sensor and the region of interest. We develop an imaging method that exploits scattering from these extra reflectors. We find that artefacts can arise in certain situations; we show how to avoid them and analyse the improvement in resolution due to the presence of waves reflected from the extra scatterers into the region of interest. We carry out the details of the analysis explicitly for the case of a single extra point reflector; the extension to more reflectors is expected to follow along similar lines.

For the scattering from point reflectors, we use an exact closed-form scattering solution [30]. For scattering from the region of interest, we use the Born (single-scattering) approximation. This approximation neglects multiple scattering within the region or object and multiple scattering between the object and its environment.

The paper is organized as follows. In section 2 we develop a mathematical model for the measured signal. We show that this signal is of the form of a Fourier integral operator applied

to a function describing the object. In section 3 we give a method for producing an image, and show that the image has the desired properties. In section 4 we discuss the fidelity of the image obtained from this method.

2. The mathematical model

The mathematical model involves a number of ingredients: (1) a model for wave propagation in free space, (2) a model for the sources and receivers, (3) exact solution for scattering from point scatterers in the foreground and (4) a (linearized) model for scattering from the scene.

2.1. A model for the wave propagation

We assume that the propagation of waves is governed by the scalar wave equation

$$\nabla^2 u - c^{-2}\ddot{u} = 0, \tag{1}$$

where the dots denote differentiation with respect to t and where $c(\boldsymbol{x})$ denotes the speed of wave propagation at $\boldsymbol{x}$. We consider the case in which objects composed of materials with varying propagation speeds are imbedded in a background medium of speed c_0.

We will use capital letters for frequency-domain quantities, which are related to time-domain quantities by the Fourier transform

$$U(\omega, \boldsymbol{x}) = \frac{1}{2\pi}\int \mathrm{e}^{\mathrm{i}\omega t} u(t, \boldsymbol{x})\,\mathrm{d}t. \tag{2}$$

We write $k = \omega/c_0$.

We consider the case in which N scattering 'centres' are present in the foreground of the scene we wish to image. These scattering centres we model as point scatterers $\delta_{z^j}(\boldsymbol{x}) = \delta(\boldsymbol{x} - \boldsymbol{z}^j)$, $j = 1, 2, \ldots, N$. If we define the field g_N to be the field due to an isotropic point source at position $\boldsymbol{y}$ and time $t = 0$, the corresponding differential equation is

$$\nabla^2_{\boldsymbol{x}} g_N(t, \boldsymbol{x}, \boldsymbol{y}) - c_0^{-2}\ddot{g}_N(t, \boldsymbol{x}, \boldsymbol{y}) - \sum_{i=1}^{N} \mu_i \delta_{z^i}(\boldsymbol{x}) g_N(t, \boldsymbol{x}, \boldsymbol{y}) = -\delta_{\boldsymbol{y}}(\boldsymbol{x})\delta(t). \tag{3}$$

Here the μ are the strengths of the point scatterers. An explicit expression for g_N is given in the next section.

Behind the cloud of scattering centres is the region or object we wish to image (see figure 1). Its propagation speed is different from c_0; we write the perturbation in wave speed as $q(\boldsymbol{x}) = c^{-2}(\boldsymbol{x}) - c_0^{-2}$.

Whether we can form a two-dimensional or three-dimensional image of the object is determined by the number of degrees of freedom in our measured data. If the data depend only on two dimensions, we expect to make only a two-dimensional image. In this case, we assume that the wave speed varies only on a known surface; we denote this known surface by $\{\boldsymbol{x} = \psi(\boldsymbol{x}_T) : \boldsymbol{x}_T \in \mathbb{R}^2\}$, where $\boldsymbol{x}_T = (x_1, x_2)$, and we write the wave speed perturbation as $q(\boldsymbol{x}_T)\delta(\boldsymbol{x} - \psi(\boldsymbol{x}_T))$. In what follows we consider for simplicity the three-dimensional case; for the two-dimensional case we would simply replace $\boldsymbol{x}$ by $\boldsymbol{x}_T$ and $q(\boldsymbol{x})$ by $q(\boldsymbol{x}_T)\delta_\psi(\boldsymbol{x} - \psi(\boldsymbol{x}_T))$.

The equation we consider can thus be written as

$$\nabla^2 u - c_0^{-2}\ddot{u} - \sum_{i=1}^{N} \mu_i \delta_{z^i} u - q\ddot{u} = 0, \tag{4}$$

where q is the quantity we wish to reconstruct.

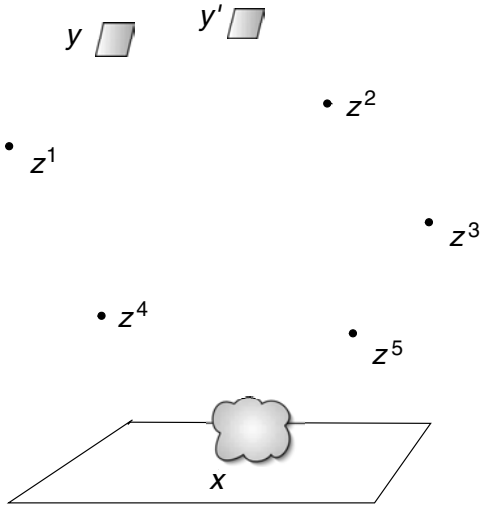

Figure 1. Scattering geometry.

2.2. A model for the sources and receivers

We model the sources and receivers as isotropic radiators. At frequency ω, the field at $\boldsymbol{x}$ emanating from the source at $\boldsymbol{y}$ is $G_0(\omega, |\boldsymbol{x} - \boldsymbol{y}|)$, where $G_0(\omega, r) = (4\pi r)^{-1} \exp(\mathrm{i}kr)$.

2.3. Multiple scattering from point scatterers

For a time-harmonic incident wave U^{in}, the frequency-domain field U^{sc} scattered from N 'point' scatterers can be obtained from the Foldy–Lax [20] or T-matrix [11, 34, 36, 37] equations together with the assumption that the scattered field from an individual 'point' scatterer is proportional to the free-space Green's function G_0 [30]:

$$U^{\mathrm{sc}}(\omega, \boldsymbol{x}) = \sum_{j=1}^{N} G_0(\omega, |\boldsymbol{x} - \boldsymbol{z}^j|)\mu_j U_j(\omega, \boldsymbol{z}^j) \tag{5}$$

$$U_j(\omega, \boldsymbol{x}) = U^{\mathrm{in}}(\omega, \boldsymbol{x}) + \sum_{i \neq j} G_0(\omega, |\boldsymbol{x} - \boldsymbol{z}^i|)\mu_i U_i(\omega, \boldsymbol{z}^i), \qquad j = 1, 2, \ldots, N. \tag{6}$$

Equation (5) says that the scattered field is the sum of the fields scattered from each scatterer; moreover, the field scattered from the jth scatterer is proportional to the field U_j that is incident upon the jth scatterer. Equations (6) say that the jth local incident field is the overall incident field plus the field scattered from all the other scatterers. If the scattering strengths $\mu_1, \mu_2, \ldots, \mu_N$ and positions $\boldsymbol{z}^1, \boldsymbol{z}^2, \ldots, \boldsymbol{z}^N$ are known, equations (6) can be solved for the U_j; then the total field $U = U^{\mathrm{inc}} + U^{\mathrm{sc}}$ can be found from (5).

The total field U satisfies the 'background' differential equation

$$\nabla^2 U + k^2 U + \sum_{i=1}^{N} \mu_i \delta_{\boldsymbol{z}^i} U = 0. \tag{7}$$

Here $k = \omega/c_0$. We note that the sense in which a field of the form (5) satisfies (7) requires an extension of the traditional distributional definition of the delta function; its domain must

be extended to include functions with $1/r$ singularities. A thorough discussion of this issue can be found in [1]; the basic ideas are outlined in appendix A.

We will write G_N for the total field U in the case when $U^{\text{inc}} = G_0$.

2.3.1. Example: a single point scatterer. For a single point scatterer of strength μ located at position $\boldsymbol{z}$, the scattered field of (5) is simply

$$U^{\text{sc}}(\boldsymbol{x}) = G_0(|\boldsymbol{x} - \boldsymbol{z}|)\mu U^{\text{in}}(\boldsymbol{z}). \tag{8}$$

The corresponding time-domain scattered field is

$$u^{\text{sc}}(t, \boldsymbol{x}) = \int \mathrm{e}^{-\mathrm{i}\omega t} G_0(\omega, |\boldsymbol{x} - \boldsymbol{z}|)\mu U^{\text{in}}(\omega, \boldsymbol{z})\, \mathrm{d}\omega. \tag{9}$$

In the case when $U^{\text{in}} = G_0$, we denote U^{sc} of (8) by G_1^{sc}. The one-point-scatterer 'background' Green's function G_1 is defined as $G_1 = G_0 + G_1^{\text{sc}}$:

$$\begin{aligned} G_1(\omega, \boldsymbol{x}, \boldsymbol{y}') &= G_0(\omega, |\boldsymbol{x} - \boldsymbol{y}'|) + G_0(\omega, |\boldsymbol{x} - \boldsymbol{z}|)\mu G_0(\omega, |\boldsymbol{z} - \boldsymbol{y}'|) \\ &= \frac{\mathrm{e}^{\mathrm{i}k|\boldsymbol{x}-\boldsymbol{y}'|}}{4\pi|\boldsymbol{x} - \boldsymbol{y}'|} + \mu \frac{\mathrm{e}^{\mathrm{i}k(|\boldsymbol{x}-\boldsymbol{z}|+|\boldsymbol{z}-\boldsymbol{y}'|)}}{(4\pi)^2|\boldsymbol{x} - \boldsymbol{z}||\boldsymbol{z} - \boldsymbol{y}'|}. \end{aligned} \tag{10}$$

We note that G_1^{sc} can be written in the form $\exp[\mathrm{i}\omega\tau(\boldsymbol{x}, \boldsymbol{y}')]A(\omega, \boldsymbol{x}, \boldsymbol{y}')$, where the travel time τ is given by $\tau = (|\boldsymbol{x} - \boldsymbol{z}| + |\boldsymbol{z} - \boldsymbol{y}'|)/c_0$ and the amplitude A is given by $A = \mu/[(4\pi)^2|\boldsymbol{x} - \boldsymbol{z}||\boldsymbol{z} - \boldsymbol{y}'|]$. We see from (10) that G_1 is the sum of two terms, the first corresponding to a direct path between $\boldsymbol{y}'$ and $\boldsymbol{x}$, and the second corresponding to a path in which the wave travels from $\boldsymbol{y}'$ to $\boldsymbol{z}$ and thence to $\boldsymbol{x}$.

2.3.2. Example: a pair of point scatterers. In the case of two point scatterers, equations (6) are

$$U_1(\boldsymbol{x}) = U^{\text{in}}(\boldsymbol{x}) + G_0(|\boldsymbol{x} - \boldsymbol{z}^1|)\mu_2 U_2(\boldsymbol{z}^2) \tag{11}$$

$$U_2(\boldsymbol{x}) = U^{\text{in}}(\boldsymbol{x}) + G_0(|\boldsymbol{x} - \boldsymbol{z}^2|)\mu_1 U_1(\boldsymbol{z}^1). \tag{12}$$

Evaluating (11) at $\boldsymbol{z}^1$ and (12) at $\boldsymbol{z}^2$ gives rise to the system of equations

$$\begin{pmatrix} 1 & -\mu_2 G_0(L) \\ -\mu_1 G_0(L) & 1 \end{pmatrix} \begin{pmatrix} U_1(\boldsymbol{z}^1) \\ U_2(\boldsymbol{z}^2) \end{pmatrix} = \begin{pmatrix} U^{\text{inc}}(\boldsymbol{z}^1) \\ U^{\text{inc}}(\boldsymbol{z}^2) \end{pmatrix}, \tag{13}$$

where $L = |\boldsymbol{z}^2 - \boldsymbol{z}^1|$. These equations have the solutions

$$U_j(\boldsymbol{z}^j) = \frac{U^{\text{inc}}(\boldsymbol{z}^j) + \mu_{j'} G_0(L) U^{\text{inc}}(\boldsymbol{z}^{j'})}{1 - \mu_1\mu_2 G_0^2(L)}, \qquad j = 1, 2, \tag{14}$$

where $j' = 2$ if $j = 1$ and $j' = 1$ if $j = 2$. Using (14) in (5) yields

$$U^{\text{sc}}(\boldsymbol{x}) = \sum_{j=1}^{2} G_0(|\boldsymbol{x} - \boldsymbol{z}^j|)\mu_j \frac{U^{\text{inc}}(\boldsymbol{z}^j) + \mu_{j'} G_0(L) U^{\text{inc}}(\boldsymbol{z}^{j'})}{1 - \mu_1\mu_2 G_0^2(L)}. \tag{15}$$

Equation (15) has a clear physical interpretation in the 'well-separated' case when $\left|\mu_1\mu_2 G_0^2(L)\right| < 1$, when we can consider the denominator to be the sum of a geometric series:

$$\begin{aligned} U^{\text{sc}}(\boldsymbol{x}) = \sum_{j=1}^{2} \Bigg[& G_0(|\boldsymbol{x} - \boldsymbol{z}^j|)\mu_j \sum_{n=0}^{\infty} \left[\mu_1\mu_2 G_0^2(L)\right]^n U^{\text{inc}}(\boldsymbol{z}^j) \\ & + G_0(|\boldsymbol{x} - \boldsymbol{z}^j|)\mu_j\mu_{j'} G_0(L) \sum_{n=0}^{\infty} \left[\mu_1\mu_2 G_0^2(L)\right]^n U^{\text{inc}}(\boldsymbol{z}^{j'}) \Bigg]. \end{aligned} \tag{16}$$

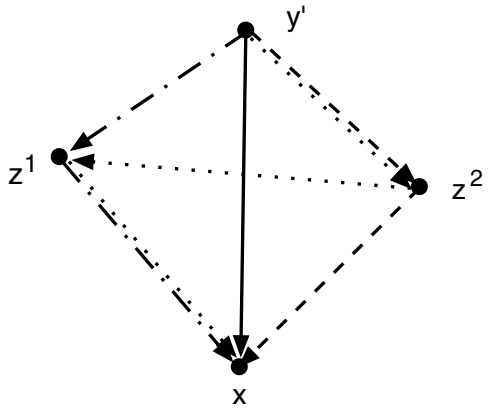

Figure 2. Paths for two point scatterers. The path 0 (corresponding to travel time τ_0^0) is shown as a solid line, path 1 as a dashed line, path 2 as a dashed-dotted line, and path 3 as a dotted line.

The $n = 0$ term on the first line of (16) corresponds to the incident wave scattering once from $\boldsymbol{z}^j$; the $n = 0$ term on the second line corresponds to the incident wave scattering once from $\boldsymbol{z}^{j'}$ and then once from $\boldsymbol{z}^j$. The $n = 1$ term on the first line corresponds to initial scattering from $\boldsymbol{z}^j$, then from $\boldsymbol{z}^{j'}$ and then from $\boldsymbol{z}^j$ again. The $n = 1$ term on the second line corresponds to initial scattering from $\boldsymbol{z}^{j'}$ and two bounces off $\boldsymbol{z}^j$. The terms corresponding to larger values of n have similar interpretations.

In any physical problem, some energy loss occurs with each bounce (modelled by the μ being less than one), so that only a few terms in the series are relevant.

If L is small enough so that $\left|\mu_1\mu_2 G_0^2(L)\right| \geqslant 1$, (15) can no longer be interpreted as a series. The situation in which $\mu_1\mu_2 G_0^2(L) \approx 1$ evidently corresponds to a resonance.

The two-point-scatterer 'background' Green's function G_2 is found by taking $U^{\mathrm{inc}} = G_0$:

$$G_2(\omega, \boldsymbol{x}, \boldsymbol{y}') = G_0(\omega, \boldsymbol{x}, \boldsymbol{y}') + \sum_{j=1}^{2} G_0(\omega, |\boldsymbol{x} - \boldsymbol{z}^j|)\mu_j \times \frac{G_0(\omega, |\boldsymbol{z}^j - \boldsymbol{y}'|) + \mu_{j'} G_0(\omega, L) G_0(\omega, |\boldsymbol{z}^{j'} - \boldsymbol{y}'|)}{1 - \mu_1\mu_2 G_0^2(\omega, L)}. \tag{17}$$

We note that when the scatterers are well separated, the interpretation (16) shows that G_2 can be written in the form

$$G_2(\omega, \boldsymbol{x}, \boldsymbol{y}') = \sum_{j \in \mathrm{paths}} \mathrm{e}^{\mathrm{i}\omega\tau_j^0(\boldsymbol{x}, \boldsymbol{y}')} A_j(\omega, \boldsymbol{x}, \boldsymbol{y}') \tag{18}$$

where τ_j^0 denotes the travel time along path j (see figure 2) and A is an amplitude that includes the geometrical spreading factors and factors of 4π, μ_1 and μ_2. In particular, we have

$$\begin{aligned} \tau_0^0 &= (|\boldsymbol{x} - \boldsymbol{y}'|)/c_0 \\ \tau_1^0 &= (|\boldsymbol{x} - \boldsymbol{z}^1| + |\boldsymbol{z}^1 - \boldsymbol{y}'|)/c_0 \\ \tau_2^0 &= (|\boldsymbol{x} - \boldsymbol{z}^2| + |\boldsymbol{z}^2 - \boldsymbol{y}'|)/c_0 \\ \tau_3^0 &= (|\boldsymbol{x} - \boldsymbol{z}^1| + L + |\boldsymbol{z}^2 - \boldsymbol{y}'|)/c_0 \end{aligned} \tag{19}$$

etc.

2.3.3. N point scatterers. When N scatterers are present, (6) is a system of N equations that can be solved by Cramer's rule, which results in a complicated but closed-form expression for the solution. This expression has a denominator containing the determinant of coefficients; this determinant has an expansion that allows for a multipath interpretation similar to that above. As before, only a limited number of terms need to be retained.

2.4. The model for scattering from the object of interest

We assume that the total field $G(\omega, \boldsymbol{y}, \boldsymbol{y}')$ at $\boldsymbol{y}$ due to the source at $\boldsymbol{y}'$ is equal to the sum of the following fields: (a) the free-space field $G_0(\omega, |\boldsymbol{y} - \boldsymbol{y}'|)$ emanating from the source, (b) the field G_N^{sc} scattered from the N point scatterers in the foreground and (c) the field G^{sc} due to an incident wave G_N scattered from the object $q(\boldsymbol{x})$. By making this assumption, we are neglecting multiple scattering between the object q and the point scatterers in the foreground. We note that neglecting multiple scattering between the object q and its environment is not necessarily a good approximation; in some cases this assumption leads to recognizable artefacts in images.

For G^{sc}, we use the *Born approximation* or *single-scattering* approximation to model the scattered field. The Born approximation in this case is

$$G_B^{\mathrm{sc}}(\omega, \boldsymbol{y}, \boldsymbol{y}') = -\int G_N(\omega, \boldsymbol{y}, \boldsymbol{x}) q(\boldsymbol{x}) G_N(\omega, \boldsymbol{x}, \boldsymbol{y}') \omega^2 \, \mathrm{d}\boldsymbol{x}. \tag{20}$$

The Born approximation makes the mapping from q to u^{sc} linear, but it is not necessarily a good approximation. Another linearizing approximation that can be used for reflection from smooth surfaces is the *Kirchhoff approximation*, in which the scattered field is replaced by its geometrical optics approximation [6, 21]. Here, however, we consider only the Born approximation.

The corresponding time-domain field is

$$g_B^{\mathrm{sc}}(t, \boldsymbol{y}, \boldsymbol{y}') = \int \mathrm{e}^{-\mathrm{i}\omega t} G_N(\omega, \boldsymbol{y}, \boldsymbol{x}) q(\boldsymbol{x}) \omega^2 G_N(\omega, \boldsymbol{x}, \boldsymbol{y}') \, \mathrm{d}\boldsymbol{x} \, \mathrm{d}\omega. \tag{21}$$

We note that this field is of the form

$$g_B^{\mathrm{sc}}(t, \boldsymbol{y}, \boldsymbol{y}') = \sum_{j \in \{\mathrm{paths}\}} F_j[q](t, \boldsymbol{y}, \boldsymbol{y}') \tag{22}$$

where

$$F_j[q](t, \boldsymbol{y}, \boldsymbol{y}') = \int \mathrm{e}^{-\mathrm{i}\omega[t - \tau_j(\boldsymbol{y}, \boldsymbol{y}', \boldsymbol{x})]} a_j(\omega, \boldsymbol{y}, \boldsymbol{y}', \boldsymbol{x}) \, \mathrm{d}\omega \, q(\boldsymbol{x}) \, \mathrm{d}\boldsymbol{x} \tag{23}$$

where τ_j denotes the travel time along path j and where a_j contains the geometrical spreading factors, scattering strengths μ_i, multiples of 4π, and (the Fourier transform of) the incident waveform. In particular,

$$\begin{aligned}
\tau_0 &= (|\boldsymbol{y} - \boldsymbol{x}| + |\boldsymbol{x} - \boldsymbol{y}'|)/c_0 \\
\tau_1 &= (|\boldsymbol{y} - \boldsymbol{x}| + |\boldsymbol{x} - \boldsymbol{z}^1| + |\boldsymbol{z}^1 - \boldsymbol{y}'|)/c_0 \\
\tau_2 &= (|\boldsymbol{y} - \boldsymbol{x}| + |\boldsymbol{x} - \boldsymbol{z}^2| + |\boldsymbol{z}^2 - \boldsymbol{y}'|)/c_0 \\
&\vdots \\
\tau_{N+1} &= (|\boldsymbol{y} - \boldsymbol{z}^1| + |\boldsymbol{z}^1 - \boldsymbol{x}| + |\boldsymbol{x} - \boldsymbol{y}'|)/c_0 \\
\tau_{N+2} &= (|\boldsymbol{y} - \boldsymbol{z}^2| + |\boldsymbol{z}^2 - \boldsymbol{x}| + |\boldsymbol{x} - \boldsymbol{y}'|)/c_0 \\
&\vdots
\end{aligned} \tag{24}$$

In summary, we are approximating the total field by $G = G_0 + G_N + G^{\mathrm{sc}} \approx G_0 + G_N + G_B^{\mathrm{sc}}$.

We note that some cases in which the background medium is attenuating can be handled by the method of [10], where the attenuation appears in the amplitudes a_j; here, however, we consider only a homogeneous, non-attenuating background medium.

3. Image formation

We outline first the strategy for the general case of N point scatterers, then carry out the detailed analysis for the case of a single point scatterer.

3.1. General strategy

We assume the source location $\boldsymbol{y}'$ and receiver location $\boldsymbol{y}$ are known; thus $G_0(\omega, \boldsymbol{y}, \boldsymbol{y}')$ can be subtracted from the received field. This leaves $G_{\mathrm{r}} = G - G_0$, which we consider to be the data in the image formation process.

The next step in the image formation process is to identify the foreground scatterers. This can be done from the early-time part (G_N) of the signal, because the scatterers are assumed to be closer to the sensors than the object of interest. Identification of the locations $\boldsymbol{z}^j$ and strengths μ_j from G_N can be done in a number of ways. One approach is to use optimization, in which one finds the z and μ that minimize

$$\min_{\boldsymbol{z}^j, \mu_j} \left\| G_N^{\mathrm{measured}} - G_N^{\mathrm{calculated}} \right\|. \tag{25}$$

Another approach for finding the locations $\boldsymbol{z}^j$ is to use Devaney's MUSIC algorithm [13]. Although the treatment in [13] is based on the Born approximation, in fact Devaney's approach applies also to the multiple-scattering case: determining the locations of the point scatterers depends only on the fact that (5) is a linear combination of the functions $G_0(\omega, |\boldsymbol{x} - \boldsymbol{z}^j|)$. A closely related method that applies in the case when the point scatterers are embedded in a weakly random medium was developed in [4, 8] and analysed in [7]. Here, however, we consider only the case in which the ambient medium is homogeneous.

Once the locations and strengths of the foreground scatterers are known, then G_N is known and can be subtracted out. This leaves G^{sc}, from which we form an image by filtered backprojection:

$$I(\boldsymbol{p}) = B[g^{\mathrm{sc}}](\boldsymbol{p}) := \sum_{j \in \{\mathrm{paths}\}} \int \mathrm{e}^{\mathrm{i}\omega[t - \tau_j(\boldsymbol{y}, \boldsymbol{y}', \boldsymbol{p})]} b_j(\omega, \boldsymbol{p}, \boldsymbol{y}, \boldsymbol{y}') g^{\mathrm{sc}}(t, \boldsymbol{y}, \boldsymbol{y}') \, \mathrm{d}\omega \, \mathrm{d}t \, \mathrm{d}\boldsymbol{y} \, \mathrm{d}\boldsymbol{y}' \tag{26}$$

where the filter b is determined below. We note that in (26), the paths are known because the foreground scatterers are known. We see below that we must take precautions to avoid artefacts in the image; in particular, we backproject only along paths that include a direct path to (or from) the scatterer.

In (26) the integration over $\boldsymbol{y}$ and $\boldsymbol{y}'$ indicates that we sum over all the data.

We illustrate the imaging process and its analysis for the case of one foreground point scatterer.

3.2. Case of a single point scatterer

For the case of a single point scatterer at position z, the Born-approximated field G_B is of the form

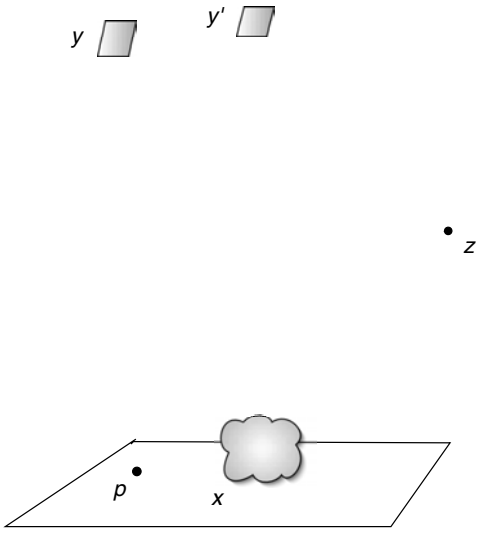

Figure 3. Geometry for forming the image. We attempt to form an image at $\boldsymbol{p}$ of the scatterer at $\boldsymbol{x}$. For an artefact-free image, we must have $\boldsymbol{p} = \boldsymbol{x}$.

$$\begin{aligned} g_B(t, \boldsymbol{y}, \boldsymbol{y}') &= g_1(t, \boldsymbol{y}, \boldsymbol{y}') + \int \mathrm{e}^{-\mathrm{i}\omega t} G_1(\omega, \boldsymbol{y}, \boldsymbol{x}) q(\boldsymbol{x}) G_1(\omega, \boldsymbol{x}, \boldsymbol{y}') \omega^2 \,\mathrm{d}\omega \,\mathrm{d}\boldsymbol{x} \\ &= g_0 + g_1^{\mathrm{sc}} + \int \mathrm{e}^{-\mathrm{i}\omega t} \big(G_0 + G_1^{\mathrm{sc}}\big) q \big(G_0 + G_1^{\mathrm{sc}}\big) \omega^2 \,\mathrm{d}\omega \,\mathrm{d}\boldsymbol{x} \\ &= g_0 + g_1^{\mathrm{sc}} + (F_1 + F_2 + F_3 + F_4)[q] \end{aligned} \tag{27}$$

where G_1 is given by (10), where $G_1^{\mathrm{sc}} = G_1 - G_0$, and where the operators F_j are

$$\begin{aligned} F_1[q](t, \boldsymbol{y}, \boldsymbol{y}') &= \int \mathrm{e}^{-\mathrm{i}\omega t} G_0(\omega, \boldsymbol{y}, \boldsymbol{x}) G_0(\omega, \boldsymbol{x}, \boldsymbol{y}') q(\boldsymbol{x}) \,\mathrm{d}\boldsymbol{x} \\ F_2[q](t, \boldsymbol{y}, \boldsymbol{y}') &= \int \mathrm{e}^{-\mathrm{i}\omega t} G_1^{\mathrm{sc}}(\omega, \boldsymbol{y}, \boldsymbol{x}) G_0(\omega, \boldsymbol{x}, \boldsymbol{y}') q(\boldsymbol{x}) \,\mathrm{d}\boldsymbol{x} \\ F_3[q](t, \boldsymbol{y}, \boldsymbol{y}') &= \int \mathrm{e}^{-\mathrm{i}\omega t} G_0(\omega, \boldsymbol{y}, \boldsymbol{x}) G_1^{\mathrm{sc}}(\omega, \boldsymbol{x}, \boldsymbol{y}') q(\boldsymbol{x}) \,\mathrm{d}\boldsymbol{x} \\ F_4[q](t, \boldsymbol{y}, \boldsymbol{y}') &= \int \mathrm{e}^{-\mathrm{i}\omega t} G_1^{\mathrm{sc}}(\omega, \boldsymbol{y}, \boldsymbol{x}) G_1^{\mathrm{sc}}(\omega, \boldsymbol{x}, \boldsymbol{y}') q(\boldsymbol{x}) \,\mathrm{d}\boldsymbol{x}. \end{aligned} \tag{28}$$

The different F correspond to different scattering paths: F_1 corresponds to the direct path τ_1 from $\boldsymbol{y}'$ to the object to $\boldsymbol{y}$; F_2 corresponds to the path τ_2 for which a wave leaves $\boldsymbol{y}'$, scatters directly from the object, then scatters off the foreground scatterer at z on its way back to $\boldsymbol{y}$; etc. (See figure 4.) Explicitly, when the F are put in the form (23), we have

$$\begin{aligned} \tau_1(\boldsymbol{y}, \boldsymbol{y}', \boldsymbol{x}) &= (|\boldsymbol{y} - \boldsymbol{x}| + |\boldsymbol{x} - \boldsymbol{y}'|)/c_0 \\ \tau_2(\boldsymbol{y}, \boldsymbol{y}', \boldsymbol{x}) &= (|\boldsymbol{y} - \boldsymbol{z}| + |\boldsymbol{z} - \boldsymbol{x}| + |\boldsymbol{x} - \boldsymbol{y}'|)/c_0 \\ \tau_3(\boldsymbol{y}, \boldsymbol{y}', \boldsymbol{x}) &= (|\boldsymbol{y} - \boldsymbol{x}| + |\boldsymbol{x} - \boldsymbol{z}| + |\boldsymbol{z} - \boldsymbol{y}'|)/c_0 \\ \tau_4(\boldsymbol{y}, \boldsymbol{y}', \boldsymbol{x}) &= (|\boldsymbol{y} - \boldsymbol{z}| + 2|\boldsymbol{x} - \boldsymbol{z}| + |\boldsymbol{z} - \boldsymbol{y}'|)/c_0. \end{aligned} \tag{29}$$

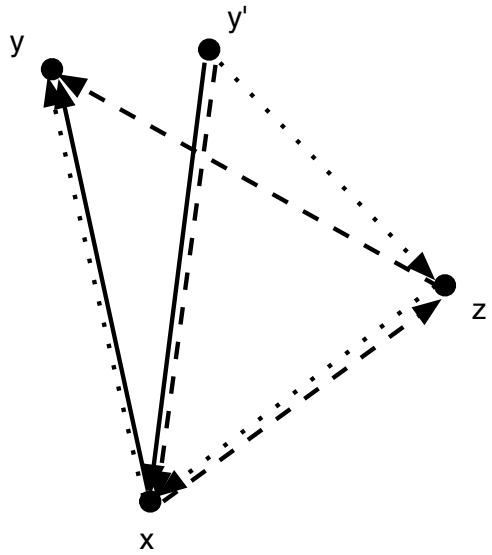

Figure 4. Paths involved in the analysis of the imaging operator. Path 1 (corresponding to travel time τ_1) is shown as a solid line, path 2 as a dashed line and path 3 as a dotted line.

3.2.1. Identification of scatterer in the foreground. We assume that the foreground point scatterers are closer to the sensor than the object q and that therefore the early-time part of (27) consists only of the term $g_1(t, \boldsymbol{y}, \boldsymbol{y}')$. Since we know $\boldsymbol{y}$ and $\boldsymbol{y}'$, we can subtract g_0 from g_1, leaving

$$g_1^{\mathrm{sc}}(t, \boldsymbol{y}, \boldsymbol{y}') = \int \mathrm{e}^{-\mathrm{i}\omega t} G_0(\omega, |\boldsymbol{y} - \boldsymbol{z}|)\mu G_0(\omega, |\boldsymbol{z} - \boldsymbol{y}'|)\,\mathrm{d}\omega$$
$$= \mu \int \frac{\mathrm{e}^{-\mathrm{i}\omega[t-(|\boldsymbol{y}-\boldsymbol{z}|-|\boldsymbol{z}-\boldsymbol{y}'|)/c_0]}}{(4\pi)^2|\boldsymbol{y} - \boldsymbol{z}||\boldsymbol{z} - \boldsymbol{y}'|}\,\mathrm{d}\omega. \tag{30}$$

In the case of a single point scatterer, there can be no multiple scattering, which implies that the field g_1 is the same as its Born approximation. We can thus form an image of the scatterer $\boldsymbol{z}$ by backprojection as described below for the $i = 1$ case.

3.2.2. Backprojection. We form the image I by means of (26). In the analysis below, we replace g^{sc} by g_B^{sc}. If, in (26), we naively backproject along all possible paths, we will see that some paths cause artefacts in the image.

Using $g^{\mathrm{sc}} \approx \sum_j F_j[q]$ (from (23)) in (26) results in an equation of the form

$$I(\boldsymbol{p}) \approx \sum_{i=1}^{4}\sum_{j=1}^{4} B_i[F_j[q]](\boldsymbol{p}) = \int K(\boldsymbol{p}, \boldsymbol{x})q(\boldsymbol{x})\,\mathrm{d}\boldsymbol{x}, \tag{31}$$

where the kernel K is the imaging *point-spread function*. If we had $K(\boldsymbol{p}, \boldsymbol{x}) = \delta(\boldsymbol{p} - \boldsymbol{x})$, then the image I would be perfect; we want to determine the b_j of (26) so that K comes as close as possible to being a delta function.

The contribution to K from $B_i F_j$ is

$$K_{i,j}(\boldsymbol{p}, \boldsymbol{x}) = \int \mathrm{e}^{\mathrm{i}\omega(t-\tau_i(\boldsymbol{y},\boldsymbol{y}',\boldsymbol{p}))} b_i(\omega, \boldsymbol{p}, \boldsymbol{y}, \boldsymbol{y}')$$
$$\times \mathrm{e}^{-\mathrm{i}\omega'(t-\tau_j(\boldsymbol{y},\boldsymbol{y}',\boldsymbol{x})} a_j(\omega', \boldsymbol{y}, \boldsymbol{y}', \boldsymbol{x})\,\mathrm{d}\omega\,\mathrm{d}\omega'\,\mathrm{d}t\,\mathrm{d}\boldsymbol{y}\,\mathrm{d}\boldsymbol{y}'. \tag{32}$$

In (32) we carry out the t and ω' integrations, obtaining

$$K_{i,j}(\boldsymbol{p},\boldsymbol{x}) = 2\pi \int \mathrm{e}^{\mathrm{i}\omega(\tau_j(\boldsymbol{y},\boldsymbol{y}',\boldsymbol{x})-\tau_i(\boldsymbol{y},\boldsymbol{y}',\boldsymbol{p}))}\, b_i(\omega,\boldsymbol{p},\boldsymbol{y},\boldsymbol{y}')\, a_j(\omega,\boldsymbol{y},\boldsymbol{y}',\boldsymbol{x})\,\mathrm{d}\omega\,\mathrm{d}\boldsymbol{y}\,\mathrm{d}\boldsymbol{y}'. \tag{33}$$

In order for K to be a close approximation to a delta function, we would like each diagonal term $K_{i,i}$ to be a good approximation to a scalar multiple of a delta function, and we would like the off-diagonal terms $K_{i,j}$, $i \neq j$, to be zero or to contribute only higher order terms. To determine whether this is the case, we analyse each term.

In each case, the analysis is similar: we use the method of stationary phase (see appendix B) to determine the leading-order contributions. Analysis of the critical points of the phase determines the locus of points $\boldsymbol{p}$ that will appear in the image due to a scatterer located at $\boldsymbol{x}$ (see figure 3). We would like the critical conditions to imply that $\boldsymbol{p} = \boldsymbol{x}$; if this is not the case, the other possible solutions $\boldsymbol{p}$ tell us which artefacts will appear in the image due to a scatterer at $\boldsymbol{x}$.

The detailed analysis of the $K_{i,j}$ is carried out in appendix C. We find that for $i \leqslant 3$, the diagonal ($i = j$) terms give rise to the desired result that $\boldsymbol{p} = \boldsymbol{x}$; this corresponds to image points that are correctly located. Some of the off-diagonal ($i \neq j$) terms can give rise to artefacts located behind the point scatterer $\boldsymbol{z}$ when viewed from either $\boldsymbol{y}$ or $\boldsymbol{y}'$. Artefacts at these locations are deemed unimportant. The term $K_{4,4}$, however, produces spherical artefacts centred at $\boldsymbol{z}$. This is because the scatterer at $\boldsymbol{z}$ is isotropic, and once a wave scatters from such a point scatterer, it loses all information about the direction from which it came. Consequently we omit the term B_4 from our backprojection operator.

Analysis of the critical conditions determines *where* in the image a scatterer at $\boldsymbol{x}$ is positioned; the coefficients b_i determine the *amplitude* of the image at $\boldsymbol{x}$. The coefficients b_i we determine from the diagonal terms $K_{i,i}$. In these diagonal terms, we make a change of variables so that the phase of $K_{i,i}$ is the phase of a delta function. Then, we determine b_i by the criterion that in order for $K_{i,i}$ to best approximate a delta function, its amplitude should be a_i such that $\sum a_i = (2\pi)^{-3}$.

3.2.3. Determination of the b_i. We have found that the imaging operator should be composed of three terms:

$$I(\boldsymbol{p}) = \sum_{i=1}^{3} B_i[g^{\mathrm{sc}}](\boldsymbol{p}) \approx \sum_{i=1}^{3}\sum_{j=1}^{4} \int K_{i,j}(\boldsymbol{p},\boldsymbol{x}) q(\boldsymbol{x})\,\mathrm{d}\boldsymbol{x} \tag{34}$$

and that moreover, if we restrict our attention to the region of interest (avoiding areas behind the scatterer at $\boldsymbol{z}$), only the diagonal terms $K_{i,i}$ contribute (to leading order) to the image. We have shown above that this imaging operator correctly positions scatterers in the region of interest.

Next we turn our attention to the scatterers' strengths, which are controlled by the factors b_i appearing in B_i. To determine the b_i, we attempt to transform each $K_{i,i}$ into a delta function. We recall that a delta function can be written as an oscillatory integral in the form $\delta(\boldsymbol{p}-\boldsymbol{x}) = (2\pi)^{-3}\int \exp[\mathrm{i}(\boldsymbol{p}-\boldsymbol{x})\cdot\boldsymbol{\xi}]\,\mathrm{d}\boldsymbol{\xi}$. Since $\boldsymbol{p}$ and $\boldsymbol{x}$ are three dimensional, we are trying to express $K_{i,i}$ as a three-dimensional integral. This means that our measured data should depend on at least three variables. This would be the case, for example, for data from an array of transducers that serve as both sources and receivers. In this case the data depend on t and two array coordinates $\boldsymbol{y}$. If more data are available, for example in the case in which we have a separate transmitting and receiving arrays, we carry out the analysis below for a three-dimensional subset of the data (say, t and the transmitter coordinates $\boldsymbol{y}$) and then simply integrate over the remaining variables.

In the exponent of (33), we use the identity

$$f(\boldsymbol{x}) - f(\boldsymbol{p}) = \int_0^1 \frac{\mathrm{d}}{\mathrm{d}\lambda} f(\boldsymbol{p} + \lambda(\boldsymbol{x} - \boldsymbol{p}))\,\mathrm{d}\lambda = (\boldsymbol{x} - \boldsymbol{p}) \cdot \int_0^1 (\nabla f)(\boldsymbol{p} + \lambda(\boldsymbol{x} - \boldsymbol{p}))\,\mathrm{d}\lambda \tag{35}$$

to write

$$\omega[\tau_i(\boldsymbol{y}, \boldsymbol{y}', \boldsymbol{x}) - \tau_i(\boldsymbol{y}, \boldsymbol{y}', \boldsymbol{p})] = (\boldsymbol{x} - \boldsymbol{p}) \cdot \Xi^i(\boldsymbol{p}, \boldsymbol{x}, \boldsymbol{y}, \boldsymbol{y}', \omega); \tag{36}$$

explicitly, the Ξ^i are given by

$$\Xi^i(\boldsymbol{p}, \boldsymbol{x}, \boldsymbol{y}, \boldsymbol{y}', \omega) = \omega \int_0^1 \nabla_{\boldsymbol{x}'} \tau_i(\boldsymbol{y}, \boldsymbol{y}', \boldsymbol{x}')\Big|_{\boldsymbol{x}' = \boldsymbol{p} + \lambda(\boldsymbol{x} - \boldsymbol{p})} \mathrm{d}\lambda; \tag{37}$$

on the right-hand side of (37), we compute the gradients of the τ_i from (29). When $\boldsymbol{p} = \boldsymbol{x}$, we have

$$\Xi^1(\boldsymbol{p}, \boldsymbol{p}, \boldsymbol{y}, \boldsymbol{y}', \omega) = k[\widehat{\boldsymbol{p} - \boldsymbol{y}} + \widehat{\boldsymbol{p} - \boldsymbol{y}'}] \tag{38}$$

$$\Xi^2(\boldsymbol{p}, \boldsymbol{p}, \boldsymbol{y}, \omega) = k[\widehat{\boldsymbol{p} - \boldsymbol{y}} + \widehat{\boldsymbol{p} - \boldsymbol{z}}] \tag{39}$$

$$\Xi^3(\boldsymbol{p}, \boldsymbol{p}, \boldsymbol{y}', \omega) = k[\widehat{\boldsymbol{p} - \boldsymbol{z}} + \widehat{\boldsymbol{p} - \boldsymbol{y}'}]. \tag{40}$$

We note that for $\boldsymbol{p} = \boldsymbol{x}$, Ξ^1 depends on both $\boldsymbol{y}$ and $\boldsymbol{y}'$, Ξ^2 is independent of $\boldsymbol{y}'$ and Ξ^3 is independent of $\boldsymbol{y}$.

In the integral (33) for $K_{1,1}$, we can make either the change of variables

$$(\omega, \boldsymbol{y}) \to \boldsymbol{\xi}^1 = \Xi^1(\boldsymbol{p}, \boldsymbol{x}, \boldsymbol{y}, \boldsymbol{y}', \omega) \tag{41}$$

or

$$(\omega, \boldsymbol{y}') \to \boldsymbol{\xi}^1 = \Xi^1(\boldsymbol{p}, \boldsymbol{x}, \boldsymbol{y}, \boldsymbol{y}', \omega); \tag{42}$$

in the integral (33) for $K_{2,2}$, we make the change of variables

$$(\omega, \boldsymbol{y}) \to \boldsymbol{\xi}^2 = \Xi^2(\boldsymbol{p}, \boldsymbol{x}, \boldsymbol{y}, \omega); \tag{43}$$

in $K_{3,3}$ we make the change of variables

$$(\omega, \boldsymbol{y}') \to \boldsymbol{\xi}^3 = \Xi^3(\boldsymbol{p}, \boldsymbol{x}, \boldsymbol{y}', \omega). \tag{44}$$

The changes of variables (41) and (43) transform expression (33) for $K_{1,1}$ and $K_{2,2}$ into

$$K_{i,i}(\boldsymbol{p}, \boldsymbol{x}) = 2\pi \int \mathrm{e}^{\mathrm{i}(p-x)\cdot\xi^i} b_i(\omega, \boldsymbol{p}, \boldsymbol{y}, \boldsymbol{y}') a_i(\omega, \boldsymbol{y}, \boldsymbol{y}', \boldsymbol{x}) \times \left| \left(\frac{\partial(\omega, \boldsymbol{y})}{\partial \boldsymbol{\xi}^i} \right) (\boldsymbol{p}, \boldsymbol{x}, \boldsymbol{y}, \boldsymbol{y}', \omega) \right| \mathrm{d}\boldsymbol{\xi}^i\, \mathrm{d}\boldsymbol{y}', \tag{45}$$

where $\boldsymbol{y} = \boldsymbol{y}(\boldsymbol{\xi})$ and $\omega = \omega(\boldsymbol{\xi})$; $K_{3,3}$ is transformed under (44) into a similar expression except that the integral is over $\boldsymbol{y}$ instead of $\boldsymbol{y}'$. (This would also be the case for $K_{1,1}$ if we had used (42) instead of (41).)

Equation (45) exhibits the point-spread function K as the kernel of a pseudodifferential operator. Pseudodifferential operators have the *pseudolocal* property [33], i.e., they do not move singularities or change their orientation. It is immediately clear from (45) that provided the Jacobian $|\partial(\omega, \boldsymbol{y})/\partial \boldsymbol{\xi}^i|$ is nonzero, the leading-order contribution to the image comes from the points $\boldsymbol{p} = \boldsymbol{x}$.

We see from (45) that the backprojection weighting functions b_i should be chosen as

$$b_i(\omega, \boldsymbol{p}, \boldsymbol{y}, \boldsymbol{y}') = \frac{\left| \left(\frac{\partial(\omega, \boldsymbol{y})}{\partial \boldsymbol{\xi}^i} \right) (\boldsymbol{p}, \boldsymbol{p}, \boldsymbol{y}, \boldsymbol{y}', \omega) \right| \chi_i(\boldsymbol{p}, \boldsymbol{y}, \boldsymbol{y}', \omega)}{(2\pi) a_i(\omega, \boldsymbol{y}, \boldsymbol{y}', \boldsymbol{p})} \tag{46}$$

where χ_i is a smooth cut-off function that prevents division by zero in (46) and that is chosen so that

$$\chi_1[\boldsymbol{p}, \boldsymbol{y}(\boldsymbol{\xi}), \boldsymbol{y}', \omega(\boldsymbol{\xi})] + \chi_2[\boldsymbol{p}, \boldsymbol{y}(\boldsymbol{\xi}), \boldsymbol{y}', \omega(\boldsymbol{\xi})] + \chi_3[\boldsymbol{p}, \boldsymbol{y}, \boldsymbol{y}'(\boldsymbol{\xi}), \omega(\boldsymbol{\xi})] = \frac{1}{(2\pi)^3} \tag{47}$$

in as large a region of $\boldsymbol{\xi}$-space (i.e., $(\omega, \boldsymbol{y})$-space) as possible. We note that in (46), $\boldsymbol{p}$ has been substituted for $\boldsymbol{x}$ in a_i and in the Jacobian determinant. This substitution results in only a lower-order (smoother) error in (45) because the leading-order contribution is from $\boldsymbol{p} = \boldsymbol{x}$.

The Jacobian determinants $|\partial(\omega, \boldsymbol{y})/\partial\boldsymbol{\xi}^i|$ are called the *Beylkin determinants* [3, 6]. They are computed from (36)–(40) as follows:

$$\frac{\partial \boldsymbol{\xi}^1}{\partial(\omega, \boldsymbol{y})} = \det\left(\frac{\widehat{\boldsymbol{p}-\boldsymbol{y}} + \widehat{\boldsymbol{p}-\boldsymbol{y}'}}{c_0} \quad -kP_{\widehat{\boldsymbol{p}-\boldsymbol{y}}}\boldsymbol{e}^1 \quad -kP_{\widehat{\boldsymbol{p}-\boldsymbol{y}}}\boldsymbol{e}^2\right) \tag{48}$$

where $P_{\boldsymbol{R}}$ is the projection operator that projects a vector onto the plane perpendicular to $\hat{\boldsymbol{R}}$:

$$P_{\boldsymbol{R}}\boldsymbol{v} = \frac{\boldsymbol{v} - \hat{\boldsymbol{R}}(\hat{\boldsymbol{R}} \cdot \boldsymbol{v})}{|\boldsymbol{R}|} \tag{49}$$

and where $\boldsymbol{e}^1$ and $\boldsymbol{e}^2$ denote unit vectors tangent to the surface of receivers. Similarly,

$$\frac{\partial \boldsymbol{\xi}^2}{\partial(\omega, \boldsymbol{y})} = \det\left(\frac{\widehat{\boldsymbol{p}-\boldsymbol{y}} + \widehat{\boldsymbol{p}-\boldsymbol{z}}}{c_0} \quad -kP_{\widehat{\boldsymbol{p}-\boldsymbol{y}}}\boldsymbol{e}^1 \quad -kP_{\widehat{\boldsymbol{p}-\boldsymbol{y}}}\boldsymbol{e}^2\right) \tag{50}$$

$$\frac{\partial \boldsymbol{\xi}^3}{\partial(\omega, \boldsymbol{y}')} = \det\left(\frac{\widehat{\boldsymbol{p}-\boldsymbol{z}} + \widehat{\boldsymbol{p}-\boldsymbol{y}'}}{c_0} \quad -kP_{\widehat{\boldsymbol{p}-\boldsymbol{y}'}}\boldsymbol{e}'^1 \quad -kP_{\widehat{\boldsymbol{p}-\boldsymbol{y}'}}\boldsymbol{e}'^2\right) \tag{51}$$

where $\boldsymbol{e}'^1$ and $\boldsymbol{e}'^2$ denote vectors tangent to the transmitting array.

The determinants of (48), (50) and (51) can be calculated easily. These determinants are nonzero because their column vectors are linearly independent: for example, the vector $\widehat{\boldsymbol{p}-\boldsymbol{y}} + \widehat{\boldsymbol{p}-\boldsymbol{y}'}$ points from the sensors towards the object, whereas $P_{\widehat{\boldsymbol{p}-\boldsymbol{y}'}}\boldsymbol{e}'^1$ and $P_{\widehat{\boldsymbol{p}-\boldsymbol{y}'}}\boldsymbol{e}'^2$ are roughly tangent to the sensor surface.

Summary. For the case of a single point scatterer in the foreground, the imaging operator should be

$$I(\boldsymbol{p}) = \sum_{j=1}^{3} B_j[g^{\mathrm{sc}}](\boldsymbol{p}) = \sum_{j=1}^{3} \int \mathrm{e}^{\mathrm{i}\omega[t-\tau_j(\boldsymbol{y},\boldsymbol{y}',\boldsymbol{p})]} b_j(\omega, \boldsymbol{p}, \boldsymbol{y}, \boldsymbol{y}')\, g^{\mathrm{sc}}(t, \boldsymbol{y}, \boldsymbol{y}')\, \mathrm{d}\omega\, \mathrm{d}t\, \mathrm{d}\boldsymbol{y}\, \mathrm{d}\boldsymbol{y}' \tag{52}$$

where the τ_j are given in (29), the b_j are chosen as in (46) and where the Jacobian determinants are given by (48), (50) and (51). We note that imaging does *not* require a lot of bookkeeping in the sense that different operators do not need to be applied to different parts of the data. Formation of the imaging operator does, however, require knowledge of the foreground scatterer and does require that the backprojection be done only along round-trip paths that include a direct one-way path between sensor and object of interest.

4. Image fidelity

With the b_i chosen as in (46), K is as close to a delta function as possible for the measurement geometry. The degree to which its leading-order term approximates a delta function is determined by the support of the χ_i, which are in turn determined through (38)–(40) by the overall size of the measurement aperture.

For the case of a single point scatterer, we determine as follows the regions in $\boldsymbol{\xi}$-space over which we have data. The image we obtain from $K_{1,1}$ is determined by the region Ω_1 in

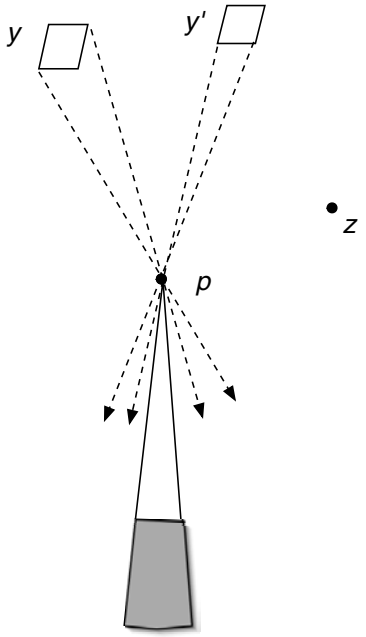

Figure 5. Region Ω_1 in Fourier space obtained from $K_{1,1}$.

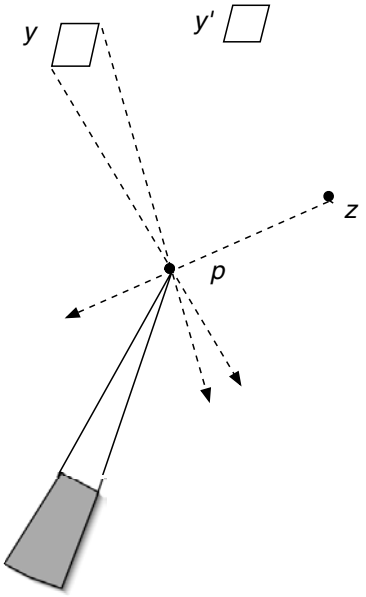

Figure 6. Region Ω_2 in Fourier space obtained from $K_{2,2}$.

Fourier space covered by the right-hand side of (38) as $\boldsymbol{y}$ and $\boldsymbol{y}'$ range over the sensors and as ω varies over the bandwidth of the transmitted waveform. This region is sketched in figure 5. The region Ω_2 we obtain from $K_{2,2}$ (sketched in figure 6) is determined by the right-hand side of (39), and the region Ω_3 obtained from $K_{3,3}$ (figure 7) is determined by the right-hand side of (40).

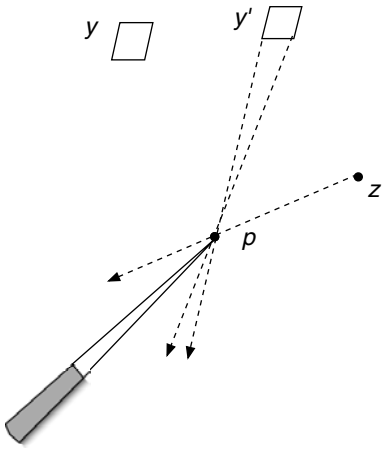

Figure 7. Region Ω_3 in Fourier space obtained from $K_{3,3}$.

The fidelity of the image obtained from the leading-order terms of the sum $K_{1,1}+K_{2,2}+K_{3,3}$ can be analysed by considering the mean-square difference between a low-pass-filtered version of the true scene q and the image I:

$$\|q_M - I\| \sim \left\| (2\pi)^{-3} \int_{B_M \setminus \cup_{i=1}^3 \Omega_i} \mathrm{e}^{\mathrm{i}\boldsymbol{\xi}\cdot(\boldsymbol{p}-\boldsymbol{x})}\, \mathrm{d}^3\boldsymbol{\xi} q(\boldsymbol{x})\, \mathrm{d}^3\boldsymbol{x} \right\| \tag{53}$$

where q_M denotes the low-pass-filtered version of q:

$$q_M(\boldsymbol{p}) = (2\pi)^{-3} \int_{B_M} \mathrm{e}^{\mathrm{i}\boldsymbol{\xi}\cdot(\boldsymbol{p}-\boldsymbol{x})} q(\boldsymbol{x})\, \mathrm{d}^3\boldsymbol{x}, \tag{54}$$

where $M = \omega_{\max}$ is the upper limit of the frequency band of the radar system, and where B_M denotes the ball $\{\boldsymbol{\xi} : |\boldsymbol{\xi}| \leqslant M\}$. To the right-hand side of (53) we apply the Cauchy–Schwartz inequality: when the Ω_i are disjoint, for example, we obtain

$$\|q_M - I\| \leqslant \frac{1}{(2\pi)^3} \left(\frac{4\pi M^3}{3} - \sum_{i=1}^{3} |\Omega_i| \right) \|q\| \tag{55}$$

where $|\Omega_i|$ denotes the volume of the set Ω_i. We see that the error (53) is decreased by subtracting the volumes of the additional sets Ω_2 and Ω_3, which are due to the multipath scattering. The precise volumes depend on the geometry, but can be obtained from (38)–(40).

We see that the L^2 notion of image fidelity depends on the size of the set $\cup\Omega_i$; this is in general agreement with the notion of resolution introduced in [35] for ultrawideband, wide-beam synthetic-aperture radar.

Similar analysis, with 'volume' replaced by 'area', applies to the case of two-dimensional imaging.

5. Conclusions

We have exhibited a backprojection imaging method that makes use of multipath scattering data from point scatterers assumed to be in the foreground of the object. We find that in order to avoid artefacts, we must backproject only along those round-trip paths that involve a direct path from object to sensor. The use of such multipath scattering improves the resulting image because it incorporates views from extra directions.

Many questions remain to be investigated. First, is it possible to apply the methods of this paper to a mathematical model that includes multiple scattering between the object and its environment [29]? What are the effects of errors in identifying the foreground point scatterers? How can the imaging algorithm best be implemented numerically?

Acknowledgments

MC thanks Cliff Nolan for helpful discussions and David Isaacson for suggesting the error measure of section 4. MC is grateful to the Air Force Office of Scientific Research and the Air Force Research Laboratory[3] for supporting this work under agreements F49620-03-1-0051 and FA87500308276. This work was also supported in part by Rensselaer Polytechnic Institute, by the UCLA Institute for Pure and Applied Mathematics, by the NSF Focused Research Groups in the Mathematical Sciences program and by CenSSIS, the Center for Subsurface Sensing and Imaging Systems, under the Engineering Research Centers Program of the National Science Foundation (award number EEC-9986821).

Appendix A. Distributional interpretation of point scatterers

We expect the differential equation

$$(\nabla^2 + k^2 + \mu\delta_z)U = 0 \tag{A.1}$$

to have solutions of the form

$$U(\boldsymbol{x}) = \phi(\boldsymbol{x}) + aG_0(|\boldsymbol{x} - \boldsymbol{z}|), \tag{A.2}$$

for some constant a, where ϕ is smooth at $\boldsymbol{x} = \boldsymbol{z}$. However, it is not obvious how the term $\delta_z U$ of (A.1) is to be interpreted, since this is not a well-defined product in the usual distribution sense. Instead, the approach of [1] is to interpret this term as $\delta_z U = \delta_z\langle\delta_z, U\rangle$, where the brackets denote the distributional action of the delta function. The key is then to extend the domain of the delta function so that it acts on functions of the form (A.2); a natural definition is for the delta function to simply ignore the singularity, so that $\langle\delta_z, \phi + aG_0(|\cdot - \boldsymbol{z}|)\rangle = \phi(\boldsymbol{z})$.

This definition results in a solution of (A.1) that is consistent with our expectations: if we use the ansatz (A.2) in (A.1), we find

$$\begin{aligned} 0 &= (\nabla^2 + k^2)(\phi + aG_0) + \mu\delta_z\langle\delta_z, \phi + aG_0\rangle \\ &= (\nabla^2 + k^2)\phi - a\delta_z + \mu\phi(\boldsymbol{z})\delta_z. \end{aligned} \tag{A.3}$$

Equating the coefficients of δ_z on both sides of (A.3), we find that $a = \mu\phi(\boldsymbol{z})$ and $(\nabla^2 + k^2)\phi = 0$. We find that the solution U is made up of a solution $\phi = U^{\text{inc}}$ to the free-space wave equation plus a scattered solution that is given by the Born approximation (8).

Appendix B. The stationary-phase theorem

The stationary-phase theorem states [5, 15, 16].

Theorem B.1. *If a is a smooth function of compact support on $\mathbf{R}^n$, and ϕ has only non-degenerate critical points, then as $\omega \to \infty$,*

[3] Consequently the US Government is authorized to reproduce and distribute reprints for Governmental purposes notwithstanding any copyright notation thereon. The views and conclusions contained herein are those of the authors and should not be interpreted as necessarily representing the official policies or endorsements, either expressed or implied, of the Air Force Research Laboratory or the US Government.

$$\int \mathrm{e}^{\mathrm{i}\omega\phi(\boldsymbol{x})} a(\boldsymbol{x})\,\mathrm{d}^n\boldsymbol{x} = \sum_{\{\boldsymbol{x}^0 : D\phi(\boldsymbol{x}^0)=\boldsymbol{0}\}} \left(\frac{2\pi}{\omega}\right)^{n/2} a(\boldsymbol{x}^0) \frac{\mathrm{e}^{\mathrm{i}\omega\phi(\boldsymbol{x}^0)}\,\mathrm{e}^{\mathrm{i}(\pi/4)\,\mathrm{sgn}D^2\phi(\boldsymbol{x}^0)}}{\sqrt{|\det D^2\phi(\boldsymbol{x}^0)|}} + O(\omega^{-n/2-1}). \tag{B.1}$$

Here $D\phi$ denotes the gradient of ϕ, $D^2\phi$ denotes the Hessian and sgn denotes the signature of a matrix, i.e., the number of positive eigenvalues minus the number of negative ones.

Appendix C. Analysis of the $K_{i,j}$

The term $K_{1,1}$. The phase of $K_{1,1}$ is

$$\begin{aligned}\phi_{1,1}(\omega, \boldsymbol{y}, \boldsymbol{y}', \boldsymbol{p}, \boldsymbol{x}) &= \omega(\tau_1(\boldsymbol{y}, \boldsymbol{y}', \boldsymbol{x}) - \tau_1(\boldsymbol{y}, \boldsymbol{y}', \boldsymbol{p})) \\ &= k[(|\boldsymbol{y} - \boldsymbol{x}| + |\boldsymbol{x} - \boldsymbol{y}'|) - (|\boldsymbol{y} - \boldsymbol{p}| + |\boldsymbol{p} - \boldsymbol{y}'|)].\end{aligned} \tag{C.1}$$

By a stationary-phase calculation, the leading-order contribution to $K_{1,1}$ comes from the stationary points at which $0 = \partial_\omega\phi_{1,1} = \partial_y\phi_{1,1} = \partial_{y'}\phi_{1,1}$. These stationary points satisfy

$$\begin{aligned} 0 &= \partial_\omega\phi_{1,1} \propto [(|\boldsymbol{y} - \boldsymbol{x}| + |\boldsymbol{x} - \boldsymbol{y}'|) - (|\boldsymbol{y} - \boldsymbol{p}| + |\boldsymbol{p} - \boldsymbol{y}'|)] \\ 0 &= \nabla_y\phi_{1,1} \propto (\widehat{\boldsymbol{y} - \boldsymbol{x}}) - (\widehat{\boldsymbol{y} - \boldsymbol{p}}) \\ 0 &= \nabla_{y'}\phi_{1,1} \propto (\widehat{\boldsymbol{x} - \boldsymbol{y}'}) - (\widehat{\boldsymbol{p} - \boldsymbol{y}'}) \end{aligned} \tag{C.2}$$

where the hats denote unit vectors. The first equation of (C.2) says that $\boldsymbol{p}$ must lie on the same equal-travel-time ellipse as $\boldsymbol{x}$; the second and third equations say that the directions from $\boldsymbol{y}$ to $\boldsymbol{x}$ and $\boldsymbol{p}$ must be the same. Clearly the only point satisifying all these conditions is $\boldsymbol{p} = \boldsymbol{x}$.

We note that the form taken by the critical conditions depends on the measurement geometry. The above analysis assumes a rather unusual situation, namely that the transmitters $\boldsymbol{y}'$ and receivers $\boldsymbol{y}$ are spread continuously over a three-dimensional region. A more common arrangement is for the sources and receivers to be spread out on a two-dimensional surface; in this case the integration in (33) is only over the two-dimensional surface of sources, and the differentiations to determine the critical points are only two dimensional. For a surface of sources and receivers, the second line of (C.2) is replaced by $(\widehat{\boldsymbol{y} - \boldsymbol{x}})_T = (\widehat{\boldsymbol{y} - \boldsymbol{p}})_T$ where the subscripts T denote the projection onto the two-dimensional surface of receivers. Similarly the third line of (C.2) is replaced by a projection onto the surface of transmitters. We note that the two-dimensional projection of a unit vector determines the unit vector in the case we have here, in which we know the unit vector is pointing downwards. (Physically the fact that the two-dimensional projection determines the unit vector corresponds to the fact that an array of sources can produce a steered beam.) Thus the critical equations for the two-dimensional array configuration imply the equations for the three-dimensional measurement geometry. For simplicity of notation, we write simply $\boldsymbol{y}$ and $\boldsymbol{y}'$ for the positions of the array elements, keeping in mind that these might vary over only a two-dimensional surface.

The term $K_{1,2}$. The phase of $K_{1,2}$ is

$$\begin{aligned}\phi_{1,2}(\omega, \boldsymbol{y}, \boldsymbol{y}', \boldsymbol{p}, \boldsymbol{x}) &= \omega(\tau_2(\boldsymbol{y}, \boldsymbol{y}', \boldsymbol{x}) - \tau_1(\boldsymbol{y}, \boldsymbol{y}', \boldsymbol{p})) \\ &= k[(|\boldsymbol{y} - \boldsymbol{z}| + |\boldsymbol{z} - \boldsymbol{x}| + |\boldsymbol{x} - \boldsymbol{y}'|) - (|\boldsymbol{y} - \boldsymbol{p}| + |\boldsymbol{p} - \boldsymbol{y}'|)].\end{aligned} \tag{C.3}$$

The stationary points satisfy

$$\begin{aligned} 0 &= \partial_\omega\phi_{1,2} \propto (|\boldsymbol{y} - \boldsymbol{z}| + |\boldsymbol{z} - \boldsymbol{x}| + |\boldsymbol{x} - \boldsymbol{y}'|) - (|\boldsymbol{y} - \boldsymbol{p}| + |\boldsymbol{p} - \boldsymbol{y}'|) \\ 0 &= \nabla_y\phi_{1,2} \propto (\widehat{\boldsymbol{y} - \boldsymbol{z}}) - (\widehat{\boldsymbol{y} - \boldsymbol{p}}) \\ 0 &= \nabla_{y'}\phi_{1,2} \propto (\widehat{\boldsymbol{x} - \boldsymbol{y}'}) - (\widehat{\boldsymbol{p} - \boldsymbol{y}'}). \end{aligned} \tag{C.4}$$

The second equation of (C.4) says that $\boldsymbol{p}$ must lie along the line joining $\boldsymbol{z}$ and $\boldsymbol{y}$. If this is the case, then $|\boldsymbol{y}-\boldsymbol{z}|-|\boldsymbol{y}-\boldsymbol{p}|=|\boldsymbol{z}-\boldsymbol{p}|$. The first equation of (C.4) then becomes

$$|\boldsymbol{z}-\boldsymbol{x}|+|\boldsymbol{x}-\boldsymbol{y}'|=|\boldsymbol{z}-\boldsymbol{p}|+|\boldsymbol{p}-\boldsymbol{y}'| \tag{C.5}$$

which shows that $\boldsymbol{p}$ must lie on the same ellipsoid as $\boldsymbol{x}$. The third equation of (C.4) specifies that $\boldsymbol{p}$ must be in the same direction from $\boldsymbol{y}'$ as $\boldsymbol{x}$; thus $\boldsymbol{p}=\boldsymbol{x}$. in other words, all conditions of (C.4) are satisfied when $\boldsymbol{p}=\boldsymbol{x}$ and $\boldsymbol{x}$ lies directly behind $\boldsymbol{z}$ when viewed from the position $\boldsymbol{y}$. This situation produces an image $\boldsymbol{p}$ of the point $\boldsymbol{x}$ in the correct position, but, because $K_{1,2}$ is an off-diagonal term, the strength of the image may be incorrect at such a location.

The term $K_{1,3}$. The phase of $K_{1,3}$ is

$$\begin{aligned}\phi_{1,3}(\omega,\boldsymbol{y},\boldsymbol{y}',\boldsymbol{p},\boldsymbol{x}) &= \omega(\tau_3(\boldsymbol{y},\boldsymbol{y}',\boldsymbol{x})-\tau_1(\boldsymbol{y},\boldsymbol{y}',\boldsymbol{p}))\\ &= k[(|\boldsymbol{y}-\boldsymbol{x}|+|\boldsymbol{x}-\boldsymbol{z}|+|\boldsymbol{z}-\boldsymbol{y}'|)-(|\boldsymbol{y}-\boldsymbol{p}|+|\boldsymbol{p}-\boldsymbol{y}'|)].\end{aligned} \tag{C.6}$$

Arguments similar to those for $K_{1,2}$ show that the only critical point occurs in the case when $\boldsymbol{x}$ is directly behind $\boldsymbol{z}$ as seen from $\boldsymbol{y}'$; in this case, the point $\boldsymbol{p}=\boldsymbol{x}$ is a critical point.

The term $K_{1,4}$. The phase of $K_{1,4}$ is

$$\begin{aligned}\phi_{1,4}(\omega,\boldsymbol{y},\boldsymbol{y}',\boldsymbol{p},\boldsymbol{x}) &= \omega(\tau_4(\boldsymbol{y},\boldsymbol{y}',\boldsymbol{x})-\tau_1(\boldsymbol{y},\boldsymbol{y}',\boldsymbol{p}))\\ &= k[(|\boldsymbol{y}-\boldsymbol{z}|+|\boldsymbol{z}-\boldsymbol{x}|+|\boldsymbol{x}-\boldsymbol{z}|+|\boldsymbol{z}-\boldsymbol{y}'|)-(|\boldsymbol{y}-\boldsymbol{p}|+|\boldsymbol{p}-\boldsymbol{y}'|)].\end{aligned} \tag{C.7}$$

The stationary points satisfy

$$\begin{aligned}0&=\partial_\omega\phi_{1,4}\propto(|\boldsymbol{y}-\boldsymbol{z}|+|\boldsymbol{z}-\boldsymbol{x}|+|\boldsymbol{x}-\boldsymbol{z}|+|\boldsymbol{z}-\boldsymbol{y}'|)-(|\boldsymbol{y}-\boldsymbol{p}|+|\boldsymbol{p}-\boldsymbol{y}'|)\\ 0&=\nabla_y\phi_{1,4}\propto(\widehat{\boldsymbol{y}-\boldsymbol{z}})-(\widehat{\boldsymbol{y}-\boldsymbol{p}})\\ 0&=\nabla_{y'}\phi_{1,4}\propto(\widehat{\boldsymbol{z}-\boldsymbol{y}'})-(\widehat{\boldsymbol{p}-\boldsymbol{y}'}).\end{aligned} \tag{C.8}$$

The last two conditions of (C.8) say that $\boldsymbol{p}$ must lie on the lines joining $\boldsymbol{y}$ to $\boldsymbol{z}$ and $\boldsymbol{y}'$ to $\boldsymbol{z}$. Unless $\boldsymbol{y}=\boldsymbol{y}'$, this implies that $\boldsymbol{p}=\boldsymbol{z}$; the first condition of (C.8) can then be satisfied only if $\boldsymbol{x}=\boldsymbol{z}$. In other words, this term can produce an artefact at the location of the foreground scatterer, which is not a location in which we are interested.

The term $K_{2,1}$. The phase of $K_{2,1}$ is the phase of $K_{1,2}$ with $\boldsymbol{y}$ and $\boldsymbol{y}'$ interchanged.

The term $K_{2,2}$. The phase of $K_{2,2}$ is

$$\begin{aligned}\phi_{2,2}(\omega,\boldsymbol{y},\boldsymbol{y}',\boldsymbol{p},\boldsymbol{x}) &= \omega(\tau_2(\boldsymbol{y},\boldsymbol{y}',\boldsymbol{x})-\tau_2(\boldsymbol{y},\boldsymbol{y}',\boldsymbol{p}))\\ &= k[(|\boldsymbol{y}-\boldsymbol{z}|+|\boldsymbol{z}-\boldsymbol{x}|+|\boldsymbol{x}-\boldsymbol{y}'|)-(|\boldsymbol{y}-\boldsymbol{z}|+|\boldsymbol{z}-\boldsymbol{p}|+|\boldsymbol{p}-\boldsymbol{y}'|)].\end{aligned} \tag{C.9}$$

The stationary points satisfy

$$\begin{aligned}0&=\partial_\omega\phi_{2,2}\propto(|\boldsymbol{y}-\boldsymbol{z}|+|\boldsymbol{z}-\boldsymbol{x}|+|\boldsymbol{x}-\boldsymbol{y}'|)-(|\boldsymbol{y}-\boldsymbol{z}|+|\boldsymbol{z}-\boldsymbol{p}|+|\boldsymbol{p}-\boldsymbol{y}'|)\\ 0&=\nabla_y\phi_{2,2}\propto(\widehat{\boldsymbol{y}-\boldsymbol{z}})-(\widehat{\boldsymbol{y}-\boldsymbol{z}})\\ 0&=\nabla_{y'}\phi_{2,2}\propto(\widehat{\boldsymbol{x}-\boldsymbol{y}'})-(\widehat{\boldsymbol{p}-\boldsymbol{y}'}).\end{aligned} \tag{C.10}$$

The second condition of (C.10) is vacuous; the third condition says that $\boldsymbol{p}$ lies on the line joining $\boldsymbol{y}'$ with $\boldsymbol{x}$. The first condition (in which the term $|\boldsymbol{y}-\boldsymbol{z}|$ cancels) says that $\boldsymbol{p}$ must lie on the same ellipsoid as $\boldsymbol{x}$. The only such point is $\boldsymbol{p}=\boldsymbol{x}$.

The term $K_{2,3}$. The phase of $K_{2,3}$ is

$$\begin{aligned}\phi_{2,3}(\omega, \boldsymbol{y}, \boldsymbol{y}', \boldsymbol{p}, \boldsymbol{x}) &= \omega(\tau_3(\boldsymbol{y}, \boldsymbol{y}', \boldsymbol{x}) - \tau_2(\boldsymbol{y}, \boldsymbol{y}', \boldsymbol{p})) \\ &= k[(|\boldsymbol{y} - \boldsymbol{x}| + |\boldsymbol{x} - \boldsymbol{z}| + |\boldsymbol{z} - \boldsymbol{y}'|) - (|\boldsymbol{y} - \boldsymbol{z}| + |\boldsymbol{z} - \boldsymbol{p}| + |\boldsymbol{p} - \boldsymbol{y}'|)].\end{aligned} \tag{C.11}$$

The stationary points satisfy

$$\begin{aligned}0 &= \partial_\omega \phi_{2,3} \propto (|\boldsymbol{y} - \boldsymbol{x}| + |\boldsymbol{x} - \boldsymbol{z}| + |\boldsymbol{z} - \boldsymbol{y}'|) - (|\boldsymbol{y} - \boldsymbol{z}| + |\boldsymbol{z} - \boldsymbol{p}| + |\boldsymbol{p} - \boldsymbol{y}'|) \\ 0 &= \nabla_y \phi_{2,3} \propto (\widehat{\boldsymbol{y} - \boldsymbol{x}}) - (\widehat{\boldsymbol{y} - \boldsymbol{z}}) \\ 0 &= \nabla_{y'} \phi_{2,3} \propto (\widehat{\boldsymbol{z} - \boldsymbol{y}'}) - (\widehat{\boldsymbol{p} - \boldsymbol{y}'}).\end{aligned} \tag{C.12}$$

The second equation of (C.12) says that $\boldsymbol{x}$ lies directly behind $\boldsymbol{z}$ when viewed from $\boldsymbol{y}$; this implies that $|\boldsymbol{x} - \boldsymbol{y}| - |\boldsymbol{y} - \boldsymbol{z}| = |\boldsymbol{z} - \boldsymbol{x}|$; similarly the third equation of (C.12) says that $\boldsymbol{p}$ lies directly behind $\boldsymbol{z}$ when viewed from $\boldsymbol{y}'$, which implies that $|\boldsymbol{z} - \boldsymbol{y}'| - |\boldsymbol{p} - \boldsymbol{y}'| = -|\boldsymbol{z} - \boldsymbol{p}|$. Thus the second and third equations of (C.12) imply that the first equation reduces to

$$2|\boldsymbol{z} - \boldsymbol{x}| = 2|\boldsymbol{z} - \boldsymbol{p}|. \tag{C.13}$$

This means that points $\boldsymbol{x}$ lying along the line joining $\boldsymbol{y}$ and $\boldsymbol{z}$ can produce artefacts along the line joining $\boldsymbol{y}'$ and $\boldsymbol{z}$. The artefact at $\boldsymbol{p}$ is at the same distance from $\boldsymbol{z}$ as the scatterer at $\boldsymbol{x}$.

The term $K_{2,4}$. The phase of $K_{2,4}$ is

$$\begin{aligned}\phi_{2,4}(\omega, \boldsymbol{y}, \boldsymbol{y}', \boldsymbol{p}, \boldsymbol{x}) &= \omega(\tau_4(\boldsymbol{y}, \boldsymbol{y}', \boldsymbol{x}) - \tau_2(\boldsymbol{y}, \boldsymbol{y}', \boldsymbol{p})) \\ &= k[(|\boldsymbol{y} - \boldsymbol{z}| + |\boldsymbol{z} - \boldsymbol{x}| + |\boldsymbol{x} - \boldsymbol{z}| + |\boldsymbol{z} - \boldsymbol{y}'|) \\ &\quad - (|\boldsymbol{y} - \boldsymbol{z}| + |\boldsymbol{z} - \boldsymbol{p}| + |\boldsymbol{p} - \boldsymbol{y}'|)].\end{aligned} \tag{C.14}$$

The stationary points satisfy

$$\begin{aligned}0 &= \partial_\omega \phi_{2,4} \propto (|\boldsymbol{y} - \boldsymbol{z}| + |\boldsymbol{z} - \boldsymbol{x}| + |\boldsymbol{x} - \boldsymbol{z}| + |\boldsymbol{z} - \boldsymbol{y}'|) - (|\boldsymbol{y} - \boldsymbol{z}| + |\boldsymbol{z} - \boldsymbol{p}| + |\boldsymbol{p} - \boldsymbol{y}'|) \\ 0 &= \nabla_y \phi_{2,4} \propto (\widehat{\boldsymbol{y} - \boldsymbol{z}}) - (\widehat{\boldsymbol{y} - \boldsymbol{z}}) \\ 0 &= \nabla_{y'} \phi_{2,4} \propto (\widehat{\boldsymbol{z} - \boldsymbol{y}'}) - (\widehat{\boldsymbol{p} - \boldsymbol{y}'}).\end{aligned} \tag{C.15}$$

The last equation of (C.15) says that $\boldsymbol{p}$ lies directly behind $\boldsymbol{z}$ when viewed from $\boldsymbol{y}'$. For such a point, we have $|\boldsymbol{z} - \boldsymbol{y}'| - |\boldsymbol{p} - \boldsymbol{y}'| = -|\boldsymbol{z} - \boldsymbol{p}|$, which converts the first equation of (C.15) into

$$2|\boldsymbol{x} - \boldsymbol{z}| = 2|\boldsymbol{z} - \boldsymbol{p}|. \tag{C.16}$$

Thus every scatterer $\boldsymbol{x}$ produces an artefact lying directly behind $\boldsymbol{z}$ when seen from $\boldsymbol{y}'$. This artefact is at the same distance from $\boldsymbol{z}$ as is $\boldsymbol{x}$.

The term $K_{3,1}$. The phase of $K_{3,1}$ is

$$\begin{aligned}\phi_{3,1}(\omega, \boldsymbol{y}, \boldsymbol{y}', \boldsymbol{p}, \boldsymbol{x}) &= \omega(\tau_1(\boldsymbol{y}, \boldsymbol{y}', \boldsymbol{x}) - \tau_3(\boldsymbol{y}, \boldsymbol{y}', \boldsymbol{p})) \\ &= k[(|\boldsymbol{y} - \boldsymbol{x}| + |\boldsymbol{x} - \boldsymbol{y}'|) - (|\boldsymbol{y} - \boldsymbol{p}| + |\boldsymbol{p} - \boldsymbol{z}| + |\boldsymbol{z} - \boldsymbol{y}'|)].\end{aligned} \tag{C.17}$$

This is the negative of the phase of $K_{1,3}$ with $\boldsymbol{x}$ and $\boldsymbol{p}$ interchanged. Again the strength of scatterers directly behind $\boldsymbol{z}$ can be incorrectly reconstructed.

The term $K_{3,2}$. The phase of $K_{3,2}$ is

$$\begin{aligned}\phi_{3,2}(\omega, \boldsymbol{y}, \boldsymbol{y}', \boldsymbol{p}, \boldsymbol{x}) &= \omega(\tau_2(\boldsymbol{y}, \boldsymbol{y}', \boldsymbol{x}) - \tau_3(\boldsymbol{y}, \boldsymbol{y}', \boldsymbol{p})) \\ &= k[(|\boldsymbol{y} - \boldsymbol{z}| + |\boldsymbol{z} - \boldsymbol{x}| + |\boldsymbol{x} - \boldsymbol{y}'|) \\ &\quad - (|\boldsymbol{y} - \boldsymbol{p}| + |\boldsymbol{p} - \boldsymbol{z}| + |\boldsymbol{z} - \boldsymbol{y}'|)].\end{aligned} \tag{C.18}$$

Again this is the negative of the phase of $K_{2,3}$ with $\boldsymbol{x}$ and $\boldsymbol{p}$ interchanged; this term can cause scatterers lying behind $\boldsymbol{z}$ from $\boldsymbol{y}$ to appear behind $\boldsymbol{z}$ when viewed from $\boldsymbol{y}'$.

The term $K_{3,3}$. The phase of $K_{3,3}$ is

$$\begin{aligned}\phi_{3,3}(\omega, \boldsymbol{y}, \boldsymbol{y}', \boldsymbol{p}, \boldsymbol{x}) &= \omega(\tau_3(\boldsymbol{y}, \boldsymbol{y}', \boldsymbol{x}) - \tau_3(\boldsymbol{y}, \boldsymbol{y}', \boldsymbol{p})) \\ &= k[(|\boldsymbol{y} - \boldsymbol{x}| + |\boldsymbol{x} - \boldsymbol{z}| + |\boldsymbol{z} - \boldsymbol{y}'|) \\ &\quad - (|\boldsymbol{y} - \boldsymbol{p}| + |\boldsymbol{p} - \boldsymbol{z}| + |\boldsymbol{z} - \boldsymbol{y}'|)]. \end{aligned} \tag{C.19}$$

The stationary points satisfy

$$\begin{aligned} 0 &= \partial_\omega \phi_{3,3} \propto (|\boldsymbol{y} - \boldsymbol{x}| + |\boldsymbol{x} - \boldsymbol{z}| + |\boldsymbol{z} - \boldsymbol{y}'|) - (|\boldsymbol{y} - \boldsymbol{p}| + |\boldsymbol{p} - \boldsymbol{z}| + |\boldsymbol{z} - \boldsymbol{y}'|) \\ 0 &= \nabla_y \phi_{3,3} \propto (\widehat{\boldsymbol{y} - \boldsymbol{x}}) - (\widehat{\boldsymbol{y} - \boldsymbol{p}}) \\ 0 &= \nabla_{y'} \phi_{3,3} \propto (\widehat{\boldsymbol{z} - \boldsymbol{y}'}) - (\widehat{\boldsymbol{z} - \boldsymbol{y}'}). \end{aligned} \tag{C.20}$$

In the first equation of (C.20), the term $|\boldsymbol{z} - \boldsymbol{y}'|$ cancels; we see that $\boldsymbol{p}$ must lie on the same ellipsoid as $\boldsymbol{x}$ and must lie in the same direction as $\boldsymbol{x}$ from $\boldsymbol{y}$. The only such point is $\boldsymbol{p} = \boldsymbol{x}$.

The term $K_{3,4}$. The phase of $K_{3,4}$ is

$$\begin{aligned}\phi_{3,4}(\omega, \boldsymbol{y}, \boldsymbol{y}', \boldsymbol{p}, \boldsymbol{x}) &= \omega(\tau_4(\boldsymbol{y}, \boldsymbol{y}', \boldsymbol{x}) - \tau_3(\boldsymbol{y}, \boldsymbol{y}', \boldsymbol{p})) \\ &= k[(|\boldsymbol{y} - \boldsymbol{z}| + 2|\boldsymbol{x} - \boldsymbol{z}| + |\boldsymbol{z} - \boldsymbol{y}'|) - (|\boldsymbol{y} - \boldsymbol{p}| + |\boldsymbol{p} - \boldsymbol{z}| + |\boldsymbol{z} - \boldsymbol{y}'|)]. \end{aligned} \tag{C.21}$$

The stationary points satisfy

$$\begin{aligned} 0 &= \partial_\omega \phi_{3,4} \propto (|\boldsymbol{y} - \boldsymbol{z}| + 2|\boldsymbol{x} - \boldsymbol{z}| + |\boldsymbol{z} - \boldsymbol{y}'|) - (|\boldsymbol{y} - \boldsymbol{p}| + |\boldsymbol{p} - \boldsymbol{z}| + |\boldsymbol{z} - \boldsymbol{y}'|) \\ 0 &= \nabla_y \phi_{3,4} \propto (\widehat{\boldsymbol{y} - \boldsymbol{z}}) - (\widehat{\boldsymbol{y} - \boldsymbol{p}}) \\ 0 &= \nabla_{y'} \phi_{3,4} \propto (\widehat{\boldsymbol{z} - \boldsymbol{y}'}) - (\widehat{\boldsymbol{z} - \boldsymbol{y}'}). \end{aligned} \tag{C.22}$$

From the second equation of (C.22), we see that $\boldsymbol{y}$, $\boldsymbol{z}$ and $\boldsymbol{p}$ all lie on the same line, which implies that $|\boldsymbol{y} - \boldsymbol{z}| - |\boldsymbol{y} - \boldsymbol{p}| = -|\boldsymbol{z} - \boldsymbol{p}|$. The first equation of (C.22) then reduces to $2|\boldsymbol{x} - \boldsymbol{z}| = 2|\boldsymbol{p} - \boldsymbol{z}|$.

Thus we see that this term can give rise to artefacts directly behind $\boldsymbol{z}$ as viewed from $\boldsymbol{y}$.

The term $K_{4,4}$.

$$\begin{aligned}\phi_{4,4}(\omega, \boldsymbol{y}, \boldsymbol{y}', \boldsymbol{p}, \boldsymbol{x}) &= \omega(\tau_4(\boldsymbol{y}, \boldsymbol{y}', \boldsymbol{x}) - \tau_4(\boldsymbol{y}, \boldsymbol{y}', \boldsymbol{p})) \\ &= k[(|\boldsymbol{y} - \boldsymbol{z}| + 2|\boldsymbol{z} - \boldsymbol{x}| + |\boldsymbol{z} - \boldsymbol{y}'|) \\ &\quad - ((|\boldsymbol{y} - \boldsymbol{z}| + 2|\boldsymbol{z} - \boldsymbol{p}| + |\boldsymbol{z} - \boldsymbol{y}'|))]. \end{aligned} \tag{C.23}$$

The stationary points satisfy

$$\begin{aligned} 0 = \partial_\omega \phi_{4,4} \propto &((|\boldsymbol{y} - \boldsymbol{z}| + |\boldsymbol{z} - \boldsymbol{x}| + |\boldsymbol{x} - \boldsymbol{z}| + |\boldsymbol{z} - \boldsymbol{y}'|) \\ &-(|\boldsymbol{y} - \boldsymbol{z}| + |\boldsymbol{z} - \boldsymbol{p}| + |\boldsymbol{p} - \boldsymbol{z}| + |\boldsymbol{z} - \boldsymbol{y}'|) \\ 0 = \nabla_y \phi_{4,4} \propto &(\widehat{\boldsymbol{y} - \boldsymbol{z}}) - (\widehat{\boldsymbol{y} - \boldsymbol{z}}) \\ 0 = \nabla_{y'} \phi_{4,4} \propto &(\widehat{\boldsymbol{z} - \boldsymbol{y}'}) - (\widehat{\boldsymbol{z} - \boldsymbol{y}'}). \end{aligned} \tag{C.24}$$

The last two equations of (C.24) are vacuous; the first equation reduces to $|\boldsymbol{x} - \boldsymbol{z}| = |\boldsymbol{p} - \boldsymbol{z}|$, which says merely that $\boldsymbol{p}$ must lie on the same travel-time sphere about $\boldsymbol{z}$ as does $\boldsymbol{x}$. In other words, backprojection of a path in which both the incident and scattered wave bounce off of $\boldsymbol{z}$ cannot be used to determine the location of a scatterer at $\boldsymbol{x}$. This is because the scatterer at $\boldsymbol{z}$ is isotropic: after a wave scatters from a point scatterer, it loses all information about the direction from which it came. In the image, this term causes spherical artefacts around $\boldsymbol{z}$; consequently we omit the term B_4 from our imaging operator, and we do not consider terms of the form $K_{4,j}$.

References

[1] Albeverio S, Gesztesy F and Hoegh-Kroem R 1988 *Solvable Models in Quantum Mechanics* (New York: Springer)

[2] Beylkin G and Burridge R 1990 Linearized inverse scattering problems in acoustics and elasticity *Wave Motion* **12** 15–52

[3] Beylkin G 1985 Imaging of discontinuities in the inverse scattering problem by inversion of a causal generalized Radon transform *J. Math. Phys.* **26** 99–108

[4] Berryman J, Borcea L, Papanicolaou G and Tsogka C 2002 Statistically stable ultrasonic imaging in random media *J. Acoust. Soc. Am.* **112** 1509–22

[5] Bleistein N and Handelsman R A 1986 *Asymptotic Expansions of Integrals* (New York: Dover)

[6] Bleistein N, Cohen J K and Stockwell J W 2000 *The Mathematics of Multidimensional Seismic Inversion* (New York: Springer)

[7] Borcea L, Papanicolaou G and Tsogka C 2003 Resolution study form imaging and time reversal in random media *Contemporary Mathematics* vol 333, ed G Alessandrini and G Uhlmann (Providence, RI: American Mathematical Society) pp 63–77

[8] Borcea L, Tsogka C, Papanicolaou G and Berryman J 2002 Imaging and time reversal in random media *Inverse Problems* **19** 1247–79

[9] Cheney M 2001 A mathematical tutorial on synthetic aperture radar *SIAM Rev.* **43** 301–12

[10] Cheney M and Nolan C J 2004 Synthetic-aperture imaging through a dispersive layer *Inverse Problems* **20** 507–32

[11] Chew W C 1990 *Waves and Fields in Inhomogeneous Media* (New York: IEEE)

[12] Duistermaat J J 1996 *Fourier Integral Operators* (Boston, MA: Birkhauser)

[13] Devaney A J 2004 Super-resolution processing of multi-static data using time reversal and MUSIC *J. Acoust. Soc. Am.* at press

[14] Devaney A J and Dennison M 2003 Inverse scattering in inhomogeneous background media *Inverse Problems* **19** 855–70

[15] Grigis A and Sjöstrand J 1994 *Microlocal Analysis for Differential Operators: An Introduction (London Mathematical Society Lecture Note Series* vol 196*)* (Cambridge: Cambridge University Press)

[16] Guillemin V and Sternberg S 1979 *Geometric Asymptotics* (Providence, RI: American Mathematical Society)

[17] Herman G T, Tuy H K, Langenberg K J and Sabatier P C 1988 *Basic Methods of Tomography and Inverse Problems* (Philadelphia, PA: Hilger)

[18] Kristensson G and Krueger R J 1987 Direct and inverse scattering in the time domain for a dissipative wave equation: III. Scattering operators in the presence of a phase velocity mismatch *J. Math. Phys.* **28** 360–70

[19] Kristensson G and Krueger R J 1989 Direct and inverse scattering in the time domain for a dissipative wave equation: IV. Use of phase velocity mismatches to simplify inversions *Inverse Problems* **5** 375–88

[20] Lax M 1951 Multiple scattering of waves *Rev. Mod. Phys.* **23** 287–310

[21] Langenberg K J, Brandfass M, Mayer K, Kreutter T, Brüll A, Felinger P and Huo D 1993 Principles of microwave imaging and inverse scattering *EARSeL Adv. Remote Sens.* **2** 163–86

[22] Louis A and Quinto E T 2000 Local tomographic methods in SONAR *Surveys on Solution Methods for Inverse Problems* ed D Colton, H W Engl, A K Louis, J R McLaughlin and W Rundell (New York: Springer)

[23] Nilsson S 1997 Application of fast backprojection techniques for some inverse problems of integral geometry *Dissertation* no 499 Linköping Studies in Science and Technology

[24] Nolan C J and Cheney M 2002 Synthetic aperture inversion *Inverse Problems* **18** 221–36

[25] Natterer F 1986 *The Mathematics of Computerized Tomography* (New York: Wiley)

[26] Nolan C J and Symes W W 1997 Global solution of a linearized inverse problem for the acoustic wave equation *Commun PDE* **22** 919–52

[27] Oppenheim A V and Shafer R W 1975 *Digital Signal Processing* (Englewood Cliffs, NJ: Prentice-Hall)

[28] Quinto E T 1993 Singularities of the X-ray transform and limited data tomography in R^2 and R^3 *SIAM J. Math. Anal.* **24** 1215–25

[29] Saillard M, Vincent P and Micolau G 2000 Reconstruction of buried objectws surrounded by small inhomogeneities *Inverse Problems* **16** 1195–208

[30] Snieder R K and Scales J A 1998 Time-reversed imaging as a diagnostic of wave and particle chaos *Phys. Rev.* E **58** 5668–75

[31] Sarkar T K, Wicks M C, Salazar-Palma M and Bonneau R J 2003 *Smart Antennas* (New York: Wiley)

[32] Treves F 1975 *Basic Linear Partial Differential Equations* (New York: Academic)

[33] Treves F 1980 *Introduction to Pseudodifferential and Fourier Integral Operators* vols I and II (New York: Plenum)

[34] Tsang L, Kong J A and Shin R T 1985 *Theory of Microwave Remote Sensing* (New York: Wiley)
[35] Ulander L M H and Hellsten H 1996 A new formula for SAR spatial resolution *AEÜ Int. J. Electron. Commun.* **50** 117–21
[36] Varadan V K and Varadan V V (ed) 1980 *Acoustic, Electromagnetic and Elastic Wave Scattering—Focus on the T-Matrix Approach* (New York: Pergamon)
[37] Waterman P C 1965 Matrix formulation of electromagnetic scattering *IEEE Proc.* **53** 805–12
[38] Ziomek L J 1985 *Underwater Acoustics: A Linear Systems Theory Approach* (Orlando, FL: Academic)